Rapid Communications | Editors' Suggestion

π-anisotropy: A nanocarbon route to hard magnetism

Timothy Moorsom,[1,*] Shoug Alghamdi,[1,2] Sean Stansill,[1] Emiliano Poli,[3] Gilberto Teobaldi,[3,4,5,6] Marijan Beg,[7,8] Hans Fangohr,[7,8] Matt Rogers,[1] Zabeada Aslam,[1] Mannan Ali,[1] B. J. Hickey,[1] and Oscar Cespedes[1,†]

[1]*School of Physics and Astronomy, University of Leeds, Leeds, LS2 9JT, United Kingdom*
[2]*Department of Physics, Taibah University, Medina, 42331, Saudi Arabia*
[3]*Scientific Computing Department, STFC-UKRI, Rutherford Appleton Laboratory, OX11 0QX Didcot, United Kingdom*
[4]*Beijing Computational Science Research Center, 100193 Beijing, China*
[5]*Stephenson Institute for Renewable Energy, Department of Chemistry, University of Liverpool, Liverpool, L69 3BX , United Kingdom*
[6]*School of Chemistry, University of Southampton, Southampton, SO17 1BJ, United Kingdom*
[7]*Faculty of Engineering and Physical Sciences, University of Southampton, Southampton, United Kingdom*
[8]*European XFEL GmbH, Holzkoppel 4, 22869 Schenefeld, Germany*

(Received 13 August 2019; revised manuscript received 11 February 2020; accepted 11 February 2020; published 28 February 2020)

High coercivity magnets are an important resource for renewable energy, electric vehicles, and memory technologies. Most hard magnetic materials incorporate rare earths such as neodymium and samarium, but concerns about the environmental impact and supply stability of these materials are prompting research into alternatives. Here, we present a hybrid bilayer of cobalt and the nanocarbon molecule C_{60} which exhibits significantly enhanced coercivity with minimal reduction in magnetization. We demonstrate how this anisotropy enhancing effect cannot be described by existing models of molecule-metal magnetic interfaces. We outline a form of anisotropy, arising from asymmetric magnetoelectric coupling in the metal-molecule interface. Because this phenomenon arises from π-d hybrid orbitals, we propose calling this effect π-anisotropy. While the critical temperature of this effect is currently limited by the rotational degree of freedom of the chosen molecule, C_{60}, we describe how surface functionalization would allow for the design of room-temperature, carbon-based hard magnetic films.

DOI: 10.1103/PhysRevB.101.060408

I. INTRODUCTION

The coupling between molecules and magnetic thin films has been intensively explored over the last 15 years. It has been observed that antiferromagnetic interface states form between a variety of organic molecules and Co or Fe films, resulting in changes to their magnetic anisotropy [1–4]. Furthermore, it has been observed that C_{60} has a profound effect on the band structure and magnetic behavior of transition metals, inducing ferromagnetic states in otherwise nonmagnetic materials [5–7]. The high electron affinity of C_{60} can overcome the work function of metals such as Au, Cu, and Co, leading to a transfer of spin polarized charge [8,9]. This interfacial coupling is accompanied by the formation of a polarized π-d hybrid interface state in the C_{60} band gap [10]. These surface interactions result in a modified density of states (DOS) at the metal surface and the formation of an antiferromagnetically (AF) coupled interface state detectable by transport and spectroscopy [11,12]. While Co/C_{60} surfaces in general exhibit increased coercivity and decreased magnetization, we observe that tuning the Co structure using a Ta seed layer leads to energy products, $\mu_0 MH$, up to 8.6 MJ/m^3, an increase of 5.2× that of uncapped Co thin films [Figs. 1(a) and 1(b)].

This increase cannot solely be explained by changes in DOS and interface hybridization. The predicted change in interface anisotropy calculated by Bairagi *et al.* in ultrathin Co films was 1.5 meV, whereas the pinning observed in Co-C_{60} films is 10.8 meV [4]. However, we propose that these effects can be explained broken interfacial symmetry. Density functional theory (DFT) simulations of the Co-C_{60} interface show that the molecule adsorbs to the surface with the atom at the vertex joining a hexagonal and pentagonal carbon ring (HP) closest to the surface. In this orientation, the sum of all p-d hybrid bonds results in a strong out-of-plane electric dipole which is dependent on the in-plane magnetization. This interfacial magnetoelectric coupling explains the dramatic increase in coercivity observed in Co-C_{60} films below the rotational transition of C_{60}.

II. MAGNETOMETRY RESULTS

Superconducting quantum interference device magnetometry results show Co/C_{60} bilayers cooled in an external field appear to exhibit exchange bias fields of up to 0.45 T and coercivity up to 1.5 T [Fig. 1(a)]. Exchange bias is commonly the result of coupling between ferromagnets (FMs) and antiferromagnets (AFs) [14]. While the Co/C_{60} interface exhibits AF coupling, this extends only for a single monolayer and the

*T.Moorsom@leeds.ac.uk
†O.Cespedes@leeds.ac.uk

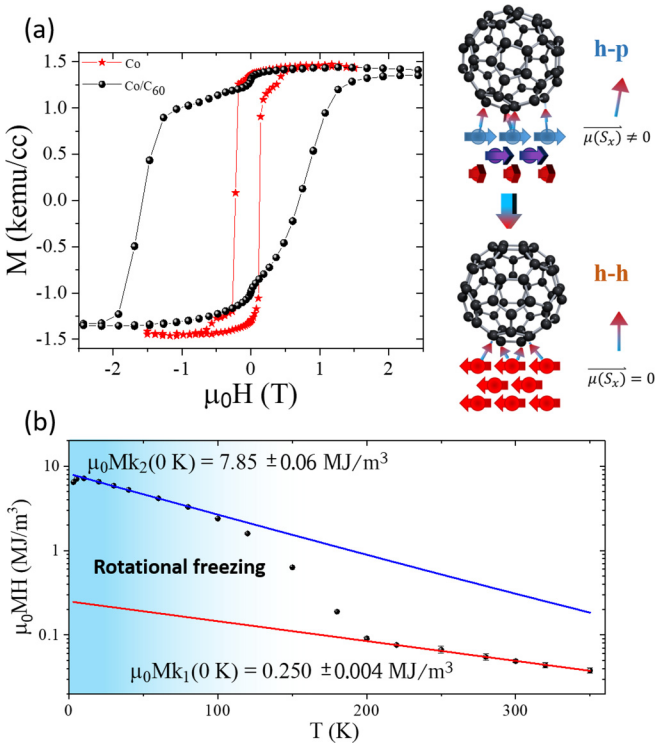

FIG. 1. (a) *MH* curves for two indentical bilayer films of Ta(4 nm)/Co(3 nm), cooled to 5 K in a 2 T applied field. The red curve (stars) is an uncapped film while the black curve (circles) is capped with a 35-nm film of C_{60}. The increase in the maximum energy product with the addition of C_{60} is 520%. The right-hand images show the expected orientation of the C_{60} molecule on the Co surface before demagnetization (top) and after (bottom). (b) The energy product for a Co/C_{60} film as a function of temperature. There are two distinct regimes above and below the rotational transition of C_{60} at 100 K. The red and blue fits are for the temperature-dependent pinning factor as described in the temperature-dependent Jiles-Atherton model, Eq. (1) [13].

C_{60} films do not show high magnetic anisotropy or exchange coupling. Furthermore, in exchange biased FM/AF bilayers, coercivity peaks at the Néel temperature of the AF due to its breakdown into weakly coupled grains which contribute to domain wall pinning but not to unidirectional anisotropy [15]. However, the temperature-dependent coercivity of these bilayers shows no such peak [Fig. 1(b)]. Analysis of the dependence of coercivity on temperature reveals two distinct regions, which can both be fit to a Jiles-Atherton (JA) model [13]. The pinning factor is roughly equivalent to coercivity and is defined as

$$k(T) = k(0)\exp\left(\frac{-2T}{\beta T_c}\right), \tag{1}$$

where k is the pinning factor, β is the critical exponent of the ferromagnet, and T_c the Curie temperature. The high-temperature region is fit to a single exponential while the low-temperature region is fit to the sum of the high-temperature behavior and a low-temperature pinning factor with differing $k(0)$ and T_c. The T_c of the high-temperature region is found to be 739 ± 6 K. While it is not possible to verify this Curie temperature in a bilayer (C_{60} evaporates at between 600 and 700 K), we expect that strong hybridization between thin-film Co and C_{60} would suppress T_c as well as saturation magnetization. The critical temperature of the low-temperature region is found to be 351 ± 9 K, well above room temperature. The steep reduction in pinning above 100 K does not fit to a JA model but shows critical behavior.

Following a single demagnetization cycle, the coercivity of the loop drops by 50% and the exchange bias is reduced to zero [Fig. 2(a)]. Changes in exchange bias after successive sweeps is observed in conventional exchange bias FM/AF bilayers where it is known as training [16]. This is typically attributed to the movement of antiferromagnetic domain walls in the AF layer. However, in this case, there is no bulk AF which might allow for the formation of AF domain walls and explain the training effect. Rather than modeling this effect according to the exchange bias model of Meiklejohn and Bean, this offset loop could be explained as the superposition of two hysteresis loops, one high coercivity and one low coercivity, of which the high coercivity loop survives only a single demagnetization cycle. It has previously been demonstrated that bilayers of hard and soft ferromagnets can produce apparently exchange biased hysteresis loops with strong training effects related to domain formation in the hard layer [17]. This model can be applied to Co/C_{60} bilayers if we consider the hybrid interface as the hard magnetic layer, which then pins the rest of the Co film. If the hard ferromagnetic layer has sufficiently high anisotropy and the soft layer is sufficiently thick, the bilayer can act as an exchange spring, in which the hysteresis loop has an entirely reversible portion at low field [18].

The first-order-reversal-curve (FORC) technique decomposes a hysteresis loop into individual demagnetization quanta or hysterons [19]. The distribution of hysterons provides information about the range of activation energies for magnetization reversal and, therefore, the variations in anisotropy, domain wall pinning, and exchange bias in a thin film. This is achieved by applying a saturating positive field followed by a nonsaturating reversal field, H_f. The sample's magnetization is then measured while sweeping the field back to positive saturation at various field setpoints, H_a. This process is repeated for progressively increasing reversal fields. The hysteron density, ρ, is then defined by the mixed second-order differential:

$$\rho(H_a, H_f) = -\frac{1}{2}\frac{d^2M}{dH_f dH_a}. \tag{2}$$

This can then be transformed into the bias field, H_b, and coercivity, H_c, using the definitions

$$H_b = \frac{H_f - H_a}{2}, \tag{3}$$

$$H_c = \frac{H_f + H_a}{2}. \tag{4}$$

The results of FORC measurements on a Co-C_{60} bilayer during the first and second sweeps are shown in Fig. 2(b). The three-dimensional (3D) plots show the hysteron density for the first and second sweeps. In the first sweep, the distribution forms a sharp peak at high bias and coercivity. Notably, the small step at zero field evident in Fig. 1(a) does not produce a hysteron peak. This is because it is completely

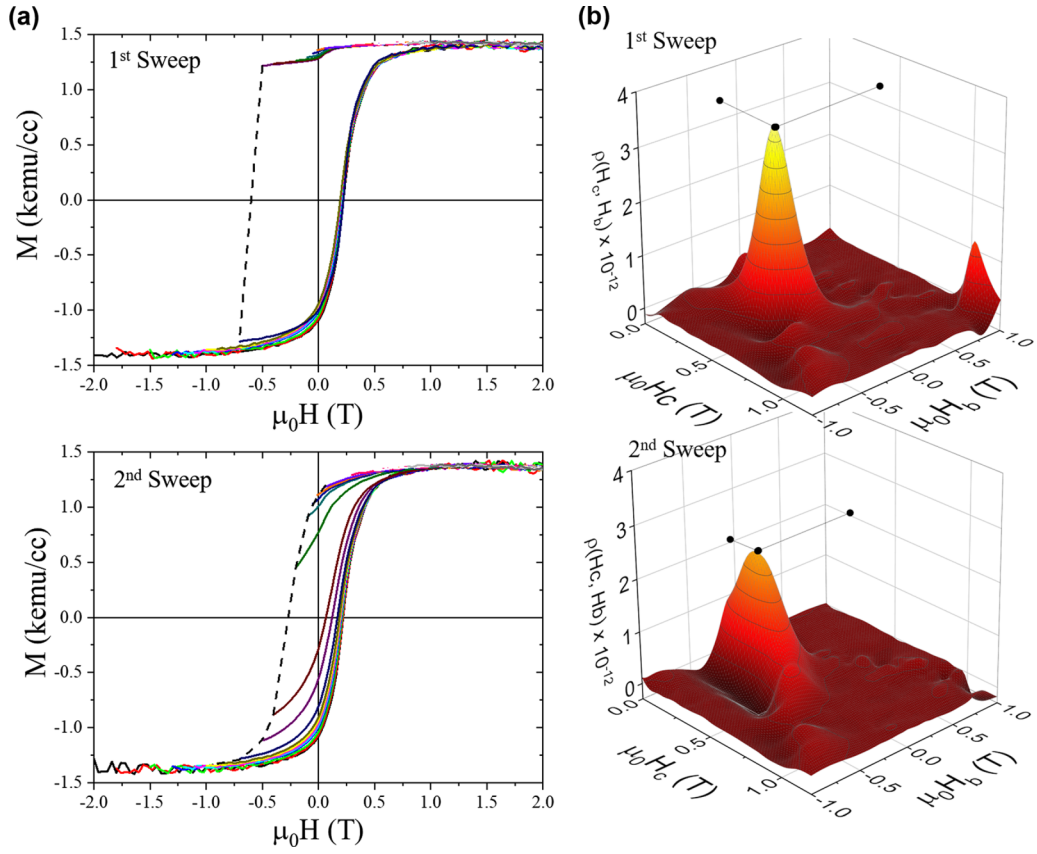

FIG. 2. (a) Minor loops for increasing values of H_a for the first and second demagnetization sweeps. (b) Hysteron density plots for the first and second demagnetization of a Co/C_{60} film cooled to 5 K in a 2 T applied field. The distribution of reversal modes is significantly changed from the first to the second sweep.

paramagnetic. In the second sweep, the hysteron peak is reduced, broadened, and pushed towards zero bias. This distribution indicates a broad range of activation energies for different reversal modes.

III. π-ANISOTROPY DISCUSSION AND SIMULATION

The transition temperature range between the high- and low-temperature regions in Fig. 1(b) corresponds closely to the range over which the rotational timescale for a C_{60} molecule is changing, with the rotation being frozen-out at 90 K in bulk films [20]. Scanning tunneling microscopy observations of single C_{60} molecules on Co, Fe, and Cr surfaces reveal that the spin polarization of the hybrid interface state is strongly dependent on interfacial symmetry, in particular in cubic metal films, where the broken interfacial symmetry gives rise to very high polarization in the fullerenes [21,22]. Our DFT simulations show that, on the (111) plane of fcc Co, the C_{60} preferentially adsorbs on the HP vertex, or 5:6 bond, leading to −6.5 eV adsorption energy and breaking of the symmetry of the interface. This leads to a symmetry-dependent interfacial spin polarization, which varies by $0.2\mu_B$ between the hexagonal and pentagonal faces of the molecule [23]. In composites containing magnetic transition metals and light elements such as carbon or oxygen, spin-orbit coupling gives rise to a spin dependence in the hybridization between p and d orbitals [24]. Where p-d hybridization occurs asymmetrically between multiple light atoms and a single transition-metal atom, this results in a spin-dependent electric dipole.

The polarization induced by spin-dependent hybridization is defined as

$$\overrightarrow{P} = \sum_{i,j}^{n,m} A_{ij}(|S_i||r_{ij}|\cos\theta_{ij})^2 \hat{r}_{ij}, \tag{5}$$

where $\vec{r}_{ij}$ is the vector pointing from a given transition-metal atom i with spin S_i, to a light atom j [25]. The angle between the bond and the spin is given as θ_{ij}. A_{ij} defines the magneto-electric coupling strength, which will primarily be dependent on spin-orbit coupling at the Co surface. At the interface between a metal lattice comprising n bonded atoms and a molecule comprising m bonded atoms, the spin-dependent contribution to the electric dipole is given by the sum of P_{ij} over all bonds.

If the molecule is bonded on the vertex between two hexagonal faces (the HH orientation), all in-plane components of the polarization in Eq. (5) will cancel. However, if it is bonded between a hexagonal and pentagonal face (HP orientation), there will be a component of $\Sigma S_{ij}^{xy} r_{ij}$ which does not cancel, due to the symmetry dependence of the hybridization, meaning an in-plane spin rotation will change the magnitude

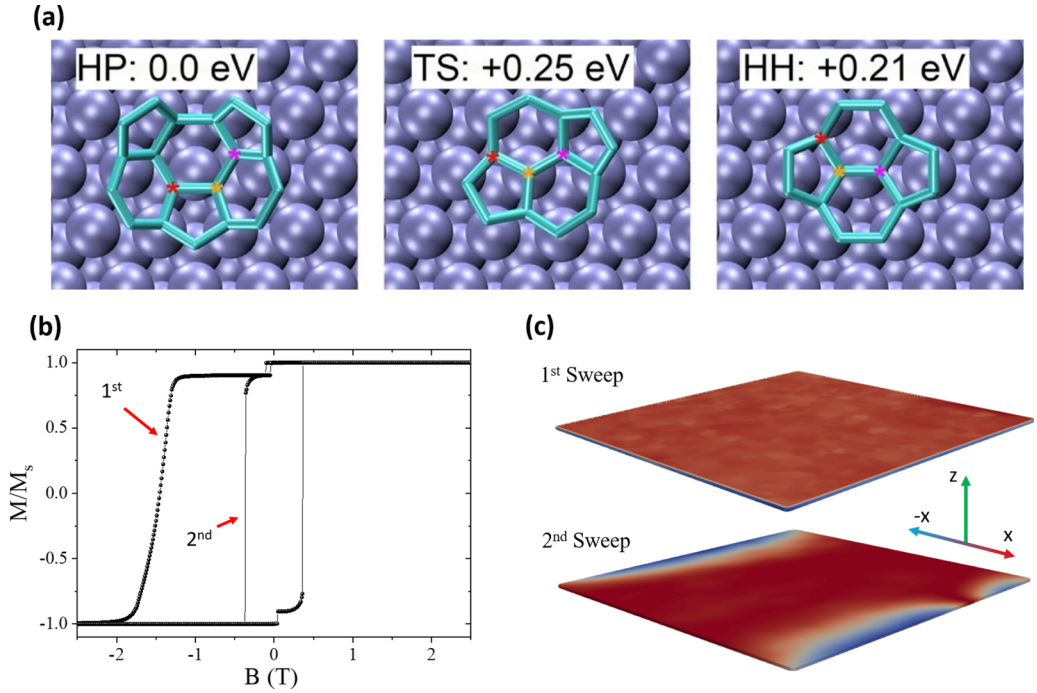

FIG. 3. (a) Representations of the Co/C_{60} stationary points during rotation as simulated via DFT. Three atoms on the hexagonal ring are marked for reference. The transition state (TS) shows the point in the HH-HP rotation where the surface energy is maximized. This is a first approximation to the energy barrier which must be overcome by the magnetoelectric torque at the interface. The C_{60} will then reach the metastable HH state. (b) Hysteresis loop simulated using the MUMAX3 code. The surface pinning replicates the vertical domain wall nucleation predicted in the π-anisotropy model. In the second sweep, this surface anisotropy is reduced, resulting in the formation of in-plane domains. (c) Shows a color map for the slab simulated in (b). Red indicates spins pointing in the $+x$ direction and blue in the $-x$ direction.

of the out-of-plane electric dipole. In addition to this spin-dependent surface dipole, there exists an in-built potential between molecule and metal due to the mismatch of Fermi levels [8]. The interaction between the spin-dependent dipole and in-built potential adds a new spin-dependent electrostatic term to the anisotropy of the Co surface.

This magnetoelectric coupling means a rotation of the in-plane spins will exert a torque on the C_{60} molecule. The observed surface exchange energy density at 3 K is 10.8 meV and the thermal energy corresponding to the center of the transition in Fig. 1(b) is 12.8 meV. DFT predicts an interfacial dipole density between a 4×4 Co(111) slab and a C_{60} molecule of $3.79 \times 10^{-3}\, e/\text{Å}$ for the HP configuration. The magnitude of the spin-dependent dipole is dependent on the magnetoelectric coupling, A_{ij}, of Co/C_{60}, which is currently unknown. However, using example values for cobalt ferrite gives a change in the spin-dependent dipole density of approximately $1 \times 10^{-6}\, e/\text{Å}$ for a 90° rotation of the surface spins of the 4×4 Co slab [26]. Despite the very high adsorption energy of the C_{60} molecule on the Co surface, DFT simulations of the transition state (TS) predict a maximum energy barrier to rotation from HP to HH of 0.25 eV [Fig. 3(a)]. This demonstrates that the energy required to rotate the C_{60} molecule on the surface is significantly lower than the adsorption energy and is likely to be further reduced in real systems due to surface defects. The C_{60} molecule will, therefore, preferentially rotate into the HH orientation as the magnetization reverses. Such spin-dependent distortions have been observed in molecule-metal interfaces using molecules such as pentacene [27]. Furthermore, Co surfaces have been observed to exhibit polarized surface states in which hybridization plays a key role in spin-orbit coupling [28]. These hybridized surface states can be directly measured via tunneling anisotropic magnetoresistance and demonstrate that coupling between magnetization direction and hybridization is a key consideration in thin films.

Once rotated, the symmetry of the HH configuration means there will be no spin-dependent dipole to rotate the molecule back into the HP configuration. The barrier for the metastable HH configuration is found from DFT to be 40 meV. While this is also likely to be lower in a real surface, this explains why the exchange bias cannot be restored without heating the bilayer above its transition temperature, at which point the C_{60} can thermally relax into the HP ground state. The superposition of high and low coercivity loops produces a similar effect to the training observed in AF/FM exchange biased bilayers, except without any actual unidirectional anisotropy [21]. This model predicts an ideal surface energy density of 32 mJ/m^2 as compared to 0.9 mJ/m^2 predicted in Co/IrMn [29]. This explains how a molecule-metal bilayer is able to produce a bias field 15× greater than that observed in Co/IrMn despite the weak interactions between magnetic molecules [15]. This also explains the unexpected temperature dependence and magnitude of this effect both as observed in Co-C_{60}, and in previous studies of molecular exchange bias [30]. Because this form of anisotropy arises from spin-dependent hybridization of molecular π orbitals, we propose calling this effect π-anisotropy.

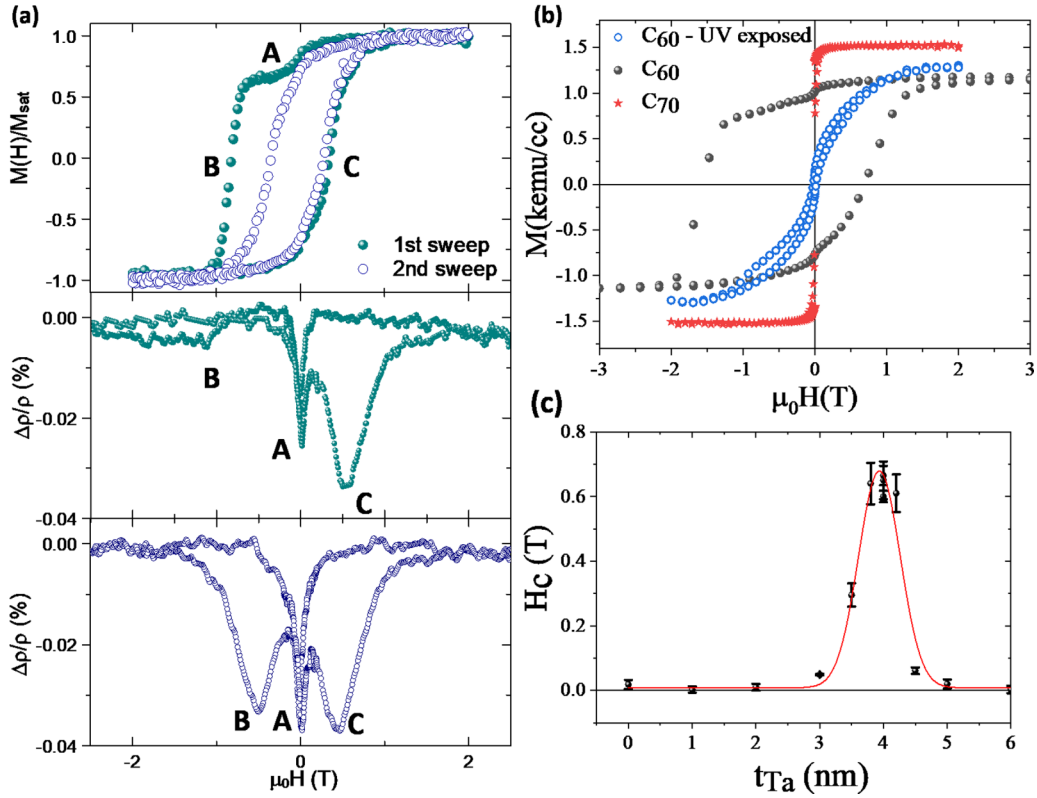

FIG. 4. (a) Top: hysteresis loops obtained from the first and second sweeps after cooling a Co/C_{60} bilayer in a 2 T applied field to 5 K. The exchange bias and asymmetry is completely destroyed after a single cycle. Middle: AMR (anisotropic magnetoresistance) recorded during the first sweep. Note that the magnetoresistance, $\Delta\rho$, is zero at point B. Bottom: AMR recorded during second sweep. Note that the AMR now exhibits expected behavior for both forward and backward sweeps. (b) Comparison of hysteresis loops at 5 K for Co/C_{60} bilayer (black circles), a Co/C_{70} bilayer (red stars), and the same Co/C_{60} bilayer after removing the molecular film with a combination of acetone and UV (blue hollow circles). (c) Dependence of the maximum recorded coercivity at 5 K on the thickness of the Ta seed layer, showing the importance of seeding the correct structure in the Co thin film.

We performed micromagnetic simulations of a Co film in contact with an antiferromagnetic layer with anisotropy $K = 27$ MJ/m^3 which simulates the surface pinning. The bottom surface of the Co film is in contact with a 3-nm paramagnetic layer which simulates a Ta/Co intermixing region. The hysteresis simulation is initialized in the positive x direction and relaxed in a 2.5-T field to simulate field cooling, varying the external magnetic field between 2.5 and -2.5 T in steps of 10 mT. We relax the system to an equilibrium state at each value of an external magnetic field and use the resulting configuration as an initial state for a new energy minimization. These simulations show coercivity of 1.5 T [Fig. 3(b)]. When the Co slab is saturated in the x direction, the anisotropy of the surface pinning layer is reduced to $K = 1$ MJ/m^3 and exchange stiffness $A = 4$ pJ/m. This simulates the depinning of the surface due to the rotation of the molecules into the symmetric HH configuration. As a result, the sweep from -2.5 to $+2.5$ T gives a coercivity of only 0.3 T and no vertical domain wall formation is observed. 3D plots of the vertical and lateral domain wall formation in the two cases are shown in Fig. 3(c). The full simulated loop replicates that observed experimentally despite the simulation having no unidirectional anisotropy.

IV. TRANSPORT RESULTS

The FORC analysis and simulations both indicate the first demagnetization occurs via an exchange spring mechansim, in which a vertical domain wall forms in the thin film which is then compressed toward a pinned interface [31]. Transport measurements support this interpretation. Hysteresis loops for a Co-C_{60} sample are shown in Fig. 4(a), with corresponding low-temperature transport data. The in-plane magnetoresistance was measured after cooling to 5 K in a 2-T applied field and performing two consecutive demagnetisation sweeps. The reversible step, point A, corresponds to the formation of a vertical domain wall, which is compressed toward the Co/C_{60} interface with increasing field. When the molecules rotate, the vertical domain wall sweeps coherently across the film producing a sharp peak in the hysteron density [Fig. 4(a)], point B. After the first demagnetization, this two-step reversal no longer occurs and there is a broader distribution of reversal modes, point C. Anisotropic magnetoresistance (AMR) measurements show a negative peak at zero field, while the first demagnetization at higher field does not feature in the AMR at all. After depinning, however, negative peaks are observed in the high field AMR for both forward and backward sweeps indicating reversal through the formation of lateral domain

walls. In magnetic thin films at low temperature, negative AMR is strongly dependent on spin scattering at domain walls, making the MR an approximate probe of the density of in-plane domain walls [32]. The lack of any change in MR during the first reversal indicates this reversal does not occur through the formation of in-plane domain walls. Molecular exchange bias has previously been observed to lead to asymmetric, negative MR in thin Co films but the explanation has until now been elusive [33].

V. STRUCTURAL DEPENDENCE

Removing C_{60} from the Co surface or using a molecule with a different symmetry does not lead to pinning. A comparison between a Co-C_{60} bilayer, a Co-C_{70} bilayer, and a Co-C_{60} layer in which the molecules have been removed using a solvent and UV exposure process is shown in Fig. 4(b). The cleaning process used to remove the molecules is summarized in the Supplemental Material [23]. Removing C_{60} from the surface results in a 98% drop in coercivity and complete removal of the exchange bias. The use of C_{70} in place of C_{60}, which is chemically almost identical but has lower symmetry, results in no pinning. Similarly, changing the structure of the Co thin film has a strong effect on the coercivity. The roughness, crystal structure, and orientation of the Co surface is strongly dependent on the seed layer. In order to produce high pinning, the Ta seed layer must be between 4 and 5 nm [Fig. 4(c)]. Ta thin films deposited on SiO_2 substrates show fcc ordering which relaxes into bcc at a certain critical thickness. This thickness is dependent on deposition temperature and material purity, but polycrystalline mixtures of bcc and fcc phases are observed above 10 nm of Ta thickness [34]. The temperature of the substrate during deposition of the bilayer was determined to be no less than 40 °C. For transition metals including Ta and Co, thin films with fcc structure strongly favor a (111) surface orientation [35]. Further details about the Ta seed layer dependence are shown in the Supplemental Material [23]. The strong dependence of the coercivity on structure and interfacial symmetry implies that further optimization of the surface properties may increase the critical temperature and magnitude of this effect.

VI. CONCLUSION

We have measured the properties of Co/C_{60} bilayers and demonstrated an extremely strong anisotropy enhancing effect arising from the C_{60} film. We have demonstrated how this anisotropy enhancing effect and resulting loop asymmetry cannot be explained by conventional models of exchange bias and surface anisotropy, indicating that molecular exchange bias is a distinct phenomenon. Nonmagnetic C_{60} is responsible for exchange springlike behavior through π-d hybridization at the interface producing a spin-dependent surface dipole which interacts with the in-built potential to create a new form of surface or π-anisotropy. Because this phenomenon would theoretically require only a single molecular layer to pin thin metal films, bilayers of this type may represent a means to create thin films and multilayers with extremely high $\mu_0 MH$ energy products. As of yet, this phenomenon is limited to low temperatures. However, we have shown evidence that the critical temperature could be much higher if it were not for the rotational degree of freedom in C_{60}. A better choice of molecule, with reduced symmetry, dopants, or ligands which prevent rotation, may produce similar or even better results at higher temperatures.

ACKNOWLEDGMENTS

This work was funded by EPSRC (Grants No. EP/I004483, No. EP/K036408, No. EPSRC EP/S030263/1, and No. EP/S031081/1), EPSRC Programme grant on Skyrmionics (Grant No. EP/N032128/1), The Horizon 2020 European Research Infrastructure project OpenDreamKit (676541), and a Taibah University Ph.D. Scholarship. This work made use of the ARCHER (via the UKCP Consortium, EPSRC UK EP/P022189/1 and EP/P022189/2), UK Materials and Molecular Modelling Hub (EPSRC UK EP/P020194/1), and STFC Scientific Computing Department's SCARF High-Performance Computing facilities.

[1] O. Cespedes, M. S. Ferreira, S. Sanvit, M. Kociak, and J. M. D. Coey, J. Phys.: Condens. Matter **16**, L155 (2004).
[2] S. Sanvito, Nat. Phys. **6**, 562 (2010).
[3] T. Moorsom, M. Wheeler, T. Mohd Khan, F. Al Ma'Mari, C. Kinane, S. Langridge, D. Ciudad, A. Bedoya-Pinto, L. Hueso, G. Teobaldi, V. K. Lazarov, D. Gilks, G. Burnell, B. J. Hickey, and O. Cespedes, Phys. Rev. B **90**, 125311 (2014).
[4] K. Bairagi, A. Bellec, V. Repain, C. Chacon, Y. Girard, Y. Garreau, J. Lagoute, S. Rousset, R. Brietwieser, Y.-C. Hu, Y. C. Chao, W. W. Pai, D. Li, A. Smogunov, and C. Barreteau, Phys. Rev. Lett. **114**, 247203 (2015).
[5] F. A. Ma'Mari, T. Moorsom, G. Teobaldi, W. Deacon, T. Prokscha, H. Luetkens, S. Lee, G. E. Sterbinsky, D. A. Arena, D. A. MacLaren, M. Flokstra, M. Ali, M. C. Wheeler, G. Burnell, B. J. Hickey, and O. Cespedes, Nature (London) **524**, 69 (2015).
[6] F. Al Ma'Mari, M. Rogers, S. Alghamdi, T. Moorsom, S. Lee, T. Prokscha, H. Luetkens, M. Valvidares, G. Teobaldi, M. Flokstra, R. Stewart, P. Gargiani, M. Ali, G. Burnell, B. J. Hickey, and O. Cespedes, Proc. Natl. Acad. Sci. USA **114**, 5583 (2017).
[7] L. Martín-Olivera, D. G. Shchukin, and G. Teobaldi, J. Phys. Chem. C **121**, 23777 (2017).
[8] X. Lu, M. Grobis, K. H. Khoo, S. G. Louie, and M. F. Crommie, Phys. Rev. B **70**, 115418 (2004).
[9] J. D. Sau, J. B. Neaton, H. J. Choi, S. G. Louie, and M. L. Cohen, Phys. Rev. Lett. **101**, 026804 (2008).
[10] C. Barraud, P. Seneor, R. Mattana, S. Fusil, K. Bouzehouane, C. Deranlot, P. Graziosi, L. Hueso, I. Bergenti, V. dediu, F. Petroff, and A. Fert, Nat. Phys. **6**, 615 (2010).
[11] K. V. Raman, A. M. Kamerbeek, A. Mukherjee, N. Atodiresei, T. K. Sen, P. Lazić, V. Caciuc, R. Michel, D. Stalke, S. K.

Mandal, S. Blügel, M. Münzenberg, and J. S. Moodera, Nature (London) **493**, 509 (2013).
[12] F. Djeghloul, M. Gruber, E. Urbain, D. Xenioti, L. Joly, S. Boukari, J. Arabski, H. Bulou, F. Scheurer, F. Bertran, P. Le Fèvre, A. Taleb-Ibrahimi, W. Wulfhekel, G. Garreau, S. Hajjar-Garreau, P. Wetzel, M. Alouani, E. Beaurepaire, M. Bowen, and W. Weber, J. Phys. Chem. Lett. **7**, 2310 (2016).
[13] A. Raghunathan, Y. Melikhov, J. E. Snyder, and D. C. Jiles, IEEE Trans. Magn. **45**, 3954 (2009).
[14] W. H. Meiklejohn and C. P. Bean, Phys. Rev. **105**, 904 (1957).
[15] M. Ali, C. H. Marrows, and B. J. Hickey, Phys. Rev. B **67**, 172405 (2003).
[16] C. Binek, Phys. Rev. B **70**, 014421 (2004).
[17] C. Binek, S. Polisetty, X. He, and A. Berger, Phys. Rev. Lett. **96**, 067201 (2006).
[18] E. F. Kneller and R. Hawig, IEEE Trans. Magn. **27**, 3588 (1991).
[19] J. E. Davies, O. Hellwig, E. E. Fullerton, J. S. Jiang, S. D. Bader, G. T. Zimanyi, and K. Liu, Appl. Phys. Lett. **86**, 262503 (2005).
[20] W. I. F. David, R. M. Ibberson, T. J. S. Dennis, J. P. Hare, and K. Prassides, Europhys. Lett. **18**, 735 (1992).
[21] S. Brems, K. Temst, and C. Van Haesendonck, Phys. Rev. Lett. **99**, 067201 (2007).
[22] D. Li, C. Barreteau, S. L. Kawahara, J. Lagoute, C. Chacon, Y. Girard, S. Rousset, V. Repain, and A. Smogunov, Phys. Rev. B **93**, 085425 (2016).
[23] See Supplemental Material at http://link.aps.org/supplemental/10.1103/PhysRevB.101.060408 for further details on sample growth, characterization, C_{60} removal, and DFT methods, which includes Refs. [30, 35–46].
[24] H. Murakawa, Y. Onose, S. Miyahara, N. Furukawa, and Y. Tokura, Phys. Rev. Lett. **105**, 137202 (2010).
[25] J. S. Lim, D. Saldana-Greco, and A. M. Rappe, Phys. Rev. B **97**, 045115 (2018).
[26] M. Etier, C. Schmitz-Antoniak, S. Salamon, H. Trivedi, Y. Gao, A. Nazrabi, J. Landers, D. Gautam, M. Winterer, D. Schmitz, H. Wende, V. V. Shvartsman, and D. C. Lupascu, Acta Mater. **90**, 1 (2015).
[27] Y.-H. Chu, C.-H. Hsu, C.-I. Lu, H.-H. Yang, T.-H. Yang, C.-H. Luo, K.-J. Yang, S.-H. Hsu, G. Hoffmann, C.-C. Kaun, and M.-T. Lin, ACS Nano **9**, 7 (2015).
[28] M. Hervé, T. Balashov, A. Ernst, and W. Wulfhekel, Phys. Rev. B **97**, 220406(R) (2018).
[29] L. Szunyogh, B. Lazarovits, L. Udvardi, J. Jackson, and U. Nowak, Phys. Rev. B **79**, 020403(R) (2009).
[30] M. Gruber, F. Ibrahim, S. Boukari, H. Isshiki, L. Joly, M. Peter, M. Studniarek, V. da Costa, H. Jabbar, V. Davesne, U. Halisdemir, J. Chen, J. Arabski, E. Otero, F. Choueikani, K. Chen, P. Ohresser, W. Wulfhekel, F. Scheurer, W. Weber, M. Alouani, E. Beaurepaire, and M. Bowen, Nat. Mater. **14**, 981 (2015).
[31] C. Pike and A. Fernandez, J. Appl. Phys. **85**, 6668 (1999).
[32] G. Tatara and H. Fukuyama, Phys. Rev. Lett. **78**, 3773 (1997).
[33] J. Jo, J. Byun, I. Oh, J. Park, M.-J. Jin, B.-C. Min, J. Lee, and J.-W. Yoo, ACS Nano **13**, 894 (2019).
[34] P. N. Denbigh and R. B. Marcus, J. Appl. Phys. **37**, 4325 (1966).
[35] J.-Y. Lee, M. Punkkinen, S. Schönecker, Z. Nabi, K. Kádas, V. Zólyomi, Y. Koo, Q.-M. Hu, R. Ahuja, B. Johansson, J. Kollár, L. Vitos, and S. Kwon, Surf. Sci. **674**, 51 (2018).
[36] L. Vitos, A. Ruban, H. Skriver, and J. Kollár, Surf. Sci. **411**, 186 (1998).
[37] C. R. Pike, A. P. Roberts, and K. L. Verosub, J. Appl. Phys. **85**, 6660 (1999).
[38] G. Kresse and J. Furthmüller, Phys. Rev. B **54**, 11169 (1996).
[39] J. P. Perdew, K. Burke, and M. Ernzerhof, Phys. Rev. Lett. **77**, 3865 (1996).
[40] M. Methfessel and A. T. Paxton, Phys. Rev. B **40**, 3616 (1989).
[41] S. L. Kawahara, J. Lagoute, V. Repain, C. Chacon, Y. Girard, S. Rousset, A. Smogunov, and C. Barreteau, Nano Lett. **12**, 4558 (2012).
[42] N. Atodiresei, J. Brede, P. Lazić, V. Caciuc, G. Hoffmann, R. Wiesendanger, and S. Blügel, Phys. Rev. Lett. **105**, 066601 (2010).
[43] J. M. López-Encarnación, J. D. Burton, E. Y. Tsymbal, and J. P. Velev, Nano Lett. **11**, 599 (2011).
[44] S. Grimme, J. Comput. Chem. **27**, 1787 (2006).
[45] G. Henkelman, B. P. Uberuaga, and H. Jónsson, J. Chem. Phys. **113**, 9901 (2000).
[46] G. Henkelman and H. Jónsson, J. Chem. Phys. **113**, 9978 (2000).